Egypt. J. Chem. **Vol. 64** No12 pp. 7621-7630 (2021)

Egyptian Journal of Chemistry

http://ejchem.journals.ekb.eg/

Studying the Physical Properties of Non-Woven Polyacrylonitrile Nano fibers after Adding γ-Fe_2O_3 Nanoparticles.

Baseem Ali Nadhim , Salih Abbas Habeeb *

Department of Polymer and Petrochemical Industries Engineering College of Materials Engineering, University of Babylon, Al Hilla –51001 ,Iraq

Abstract

This research focuses on preparing and studying the behavior of non-woven polyacrylonitrile (PAN) nanofibers after adding γ-Fe_2O_3 nanoparticles to (PAN / N, N dimethylformamide (DMF)) solution with (1.45, 4.3, and 7.14) wt. %. In order to achieve the morphology properties, textural directionality, the bonding between iron oxide particles and the PAN matrix, thermal, crystalline, and magnetic properties we did the Field-Emission Scanning Electron Microscopy (FE-SEM), Fourier Transform Near-Infrared Spectroscopy (FT-NIR), Differential Calorimeter Scanning (DSC), X-Ray Diffraction (XRD), and Vibration Sample Magnetometer (VSM). Laboratory analyses demonstrated the significant influence of iron oxide nanoparticles on the characteristics and performance of the composite nanofibers in terms of reduced nanofiber diameter from 109.38±29.70 to 78.17±36.898 nm, the disappearance of beads. In addition to an increase in the crystallinity from 82.43 to 94.28 % accompanied by a larger crystalline size as a result of the polymeric fibers acquiring high magnetic properties after strengthening them with iron oxide nanoparticles, the saturation magnetization (Ms) increases with the increase of iron oxide loading in the nanofibers from (1.426 emu/g) at 1.45 wt.% γ- Fe_2O_3 to (6.85 emu/g) to 7.14 wt.% γ- Fe_2O_3 .

Key Words: γ- Fe_2O_3 nanoparticles; Texture direction; Saturation magnetization; Glass transition temperature; polyacrylonitrile nanofibers ; Crystallinity percentage

1. Introduction

The achievements of current nanofiber technology are one of the most important goals of modern research, which is produced by the electrospinning technique that allows the preparation of non-woven fibrous materials with distinct morphological properties such as fine diameters, high gas permeability [1-4], small fibrous pore sizes, large surface-to-volume ratio, highly disciplined porosity, and flexibility [5-8] .

The diversity of uses polyacrylonitrile is considerable especially in engineering applications due to the thermal stability, mechanical properties, and chemical resistance of this material [9]. In addition, widely used this material as a matrix in polymer nanocomposites in its engineering potential applications due to its ease of processing. Furthermore, the manufacturing cost is low, and the magnetic properties are particularly notable, such as the giant magnetism resistance (GMR) in which a magnetic material can be produced from non-magnetic possessing [10], advantages in the physical and chemical properties achieved when hardening the polymer matrix with inorganic fillers such as Fe_2O_3 [10,11]. Fe_2O_3 nanoparticles are very important in application areas such as catalysis, pigmentation, and sensors. The properties of these particles such as crystal size, surface area to volume ratio, and temperature of growth are important in these applications [12] . Park, et al. studied the effect of iron oxide particle concentration and magnetic field strength in controlling the rate of bead formation and thermal stability of composite nanofibers compared to pure polyurethane nanofibers [13].

Zhang, et al. explained that Fe_2O_3 nanoparticles enhanced the adhesion between the nanofibers and increase their mechanical friction; in addition to that, iron particles with titanium dioxide particles make the nanofibers produced more flexible [11]. On the other hand, adding metal oxides leads to an increase in the shear rate and shear viscosity due to an increase in the magnetic field resulting from the presence of these particles [14, 15].

*Corresponding author e-mail: drsaleh.abbas@uobabylon.edu.iq ; ORCID: https://orcid.org/0000-0003-4687-1744
Receive Date: 05 May 2021, Revise Date: 10 July 2021, Accept Date: 13 July 2021
DOI: 10.21608/EJCHEM.2021.75271.3694

Moreover, the thermal and rheological properties of polymeric solution are dependent on the controlling the Fe_2O_3 nanoparticle concentrations' to change the viscosity of a fluid as the thickener or thinning shear rate [16, 17]. The morphological properties of composite nanofibers such as alignment of nanofibers are dependent on the metal oxide nanoparticle, because the superparamagnetism behavior and high fluorescence intensity increased with raising the amounts of metal oxide [18]. Beside, these nanoparticles gave uniform nanoporous network, high electric conductivity, and structural stability [19].
The aim of the research is to prepare 3-D composite nanofibers from PAN and iron oxide nanoparticles with no aggregates and higher dispersion of γ- Fe_2O_3 nanoparticles in the polymer matrix, which led to producing a uniform nanoporous fabric with highly aligned, low nanofibers diameter, high thermal, crystalline, and magnetic characteristics.

2. Experimental Section

2.1 Materials

The Sigma-Aldrich –Germany, supplied commercial PAN powder with a molecular weight of 100 000 g /mol , and 50 micron average particle size . N,N dimethylformamide (DMF, 99.7%) was purchased from ALPHA CHEMIKA-India . Iron Oxide Nanopowder (γ- Fe_2O_3 , gamma, 99%, 20-40 nm), Stock# : US3210 , CAS # : 1309-37-1 supplied from US Research Nanomaterials , Inc (3302 Twig Leaf Ln , Houston , TX77084,USA) .

2.2 Preparation of polymer solution and nanofibers fabrication

2.2.1 Preparation of polymer solution

The PAN: DMF solutions with polymer loading of 7.0 wt.% were prepared by added the suitable amount from PAN powder to DMF solvent and continues mixing by a magnetic stirrer with the heating temperature doesn't access 40 ˚C until completed dissolving all PAN powder and obtaining a homogeneous solution, then sonicated the polymeric solution for 10 minutes. On the other hand, the composite polymeric solutions were prepared by added the suitable weight percentages from iron oxide as 1.45, 4.3, and 7.14 wt. % to 7.0 wt. % PAN: DMF solutions. Then continued with heated at a temperature of under 40 ˚C with mechanical mixing by using the glass rod until the dispersion of the iron oxide nanoparticles in the polymer matrix and getting the homogeneous solution, then sonicated the solution produced for 40 minutes to complete the dispersion of nanoparticles in the PAN: DMF solution.

2.2.2 Nanofibers Fabrication

Pure PAN and PAN:γ- Fe_2O_3 nanocomposite fibers were prepared by using an electrospinning method. The viscous polymer solutions were loaded in a 1 ml syringe equipped with a 0.60 mm (inner diameter) stainless steel gauge needle. The grounded counter electrode was a flat aluminum foil. The solution was controllably supplied using an (MS-2200-Daiwha syringe infusion pump). The feed rate was controlled at 1.0 ml/ hr. In this work, the applied voltage was controlled at 20 kV and the rotational speed of the collector was controlled at 600 rpm. An external electric field with a high voltage applied to the polymer solution through the positive electrode can overcome the surface tension of the viscous polymer solution and form a polymer jet, then accelerates toward the rotary collector and forms the nanofibers. The preparation solutions and electrospinning process can be seen in Fig .1

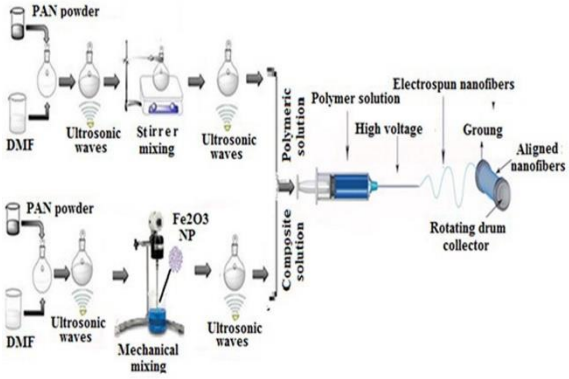

Fig.1 Schematic diagram of the solution preparation steps and the electro spinning process.

2.3 Characterizations.

The morphology (size, shape and diameter) of the pure PAN and PAN:γ- Fe_2O_3 nanocomposite fibers was evaluated using field-emission scanning electron microscopy (FE-SEM) (MIRA3 TESCAN-FRANCE). Topography and other properties of surfaces can be determined with atomic force microscopy (AFM) technique by using the Scanning Prope Microscopy (SPM- AA3000). UV- Visible spectrophotometer is used, type UV-1800, (Shimadzu-Japan) and Fourier transform Near-infrared spectroscopy (Spectrum Two N™ FT-NIR, PerkinElmer, Inc.-USA) was used to characterize the electrospun pure PAN and PAN: γ- Fe_2O_3 nanocomposite fibers. The crystal structure of the pure

PAN and nanocomposite fibers were investigated by the X-Ray Diffraction (Philips PAN alytical –X'Pert High Score Plus) at room temperature, and used the [X-Ray Tube: Cu (Kα= 1.54060 Å), Generator Settings: 30 mA, at 40 kV, and 2θ = 9.9250 º - 80.0750º, Step Size (°2Th.): 0.0500.]. The differential calorimeter scanning (Netzsch DSC 204 F1) was used to test the thermal properties of nanofibers by heating 5 mg from samples tested at a 10 ˚C / min scanning rate under the argon pressure. The average error of thermal effects was ± 3 %, a temperature range of 50–400 ˚C, and melting enthalpy was calculated using the NETZSCH Proteus program. On the other hand, the magnetic properties of nanofibers was tested by Vibration Sample Magnetometer (VSM) system (PPMS, Quantum Design), and the external field range was limited from -15,000 to 15,000 Oe at 27 ° C.

3. Results and Discussion

3.1 Morphological and Surface Properties

To determine the accuracy of the results of the morphological properties of the pure PAN nanofibers such as diameter, amount of beads formed, besides the high orientation, and compare them with the results of the morphological properties of the nanofibers reinforced with a different weight percentage of γ-Fe_2O_3 nanoparticles. Must be used the high-resolution field-emission scanning electron microscopy (FE-SEM) with a magnification power of 200 nm. On the other hand, the mean, standard deviation (SD) diameter, and nanofibers diameter ranges were calculated using the Digitizer Image Analysis Software program.

In addition, diameter distribution histograms were plotted using QI Macros (SPC Software for Excel, Six Sigma Software) as shown in Fig.2. Through this figure, we notice the clear effect of iron oxide nanoparticles on the size and numbers of the formed beads, as they begins to disappear with the increase in the weight percentage of these particles (Fig. 2a). In addition there was a decrease in the diameter of the nanofiber from (109.38± 29.702 nm) to (78.17± 36.898 nm) and the decrease in the range from (155.836-55.096 nm) in the case of the pure PAN nanofiber to (153.710-24.304 nm) in the case of the composite nanofiber.

The distribution of the nanofibers diameter appears gradually narrowing because of the decrease in the diameter of the fiber and the distances between the nanofibers, which leads to a change in the pore size. This result gives an important impression that the surface area to volume and the porosity % are improving (Fig. 2b). This result was reported in the previous study [20, 21]. According to the SPM imager surface roughness of 3D and 2D- micrographs AFM images we note that the change in the surface properties of the composite nanofibers such as average surface roughness (Ra), root mean square surface roughness (Rq), peak-to-valley roughness of the scanned region (Rpv), and surface area ratio (Sdr) compared to the surfaces of the pure nanofibers . Fig. 3 indicates an increase in the surface roughness of the AFM images of the composite nanofibers compared to the surface roughness of the pure nanofibers, these results are listed in Table 1.The higher surface roughness led to improvements in the contact angle of web nanofibers [22, 23] .

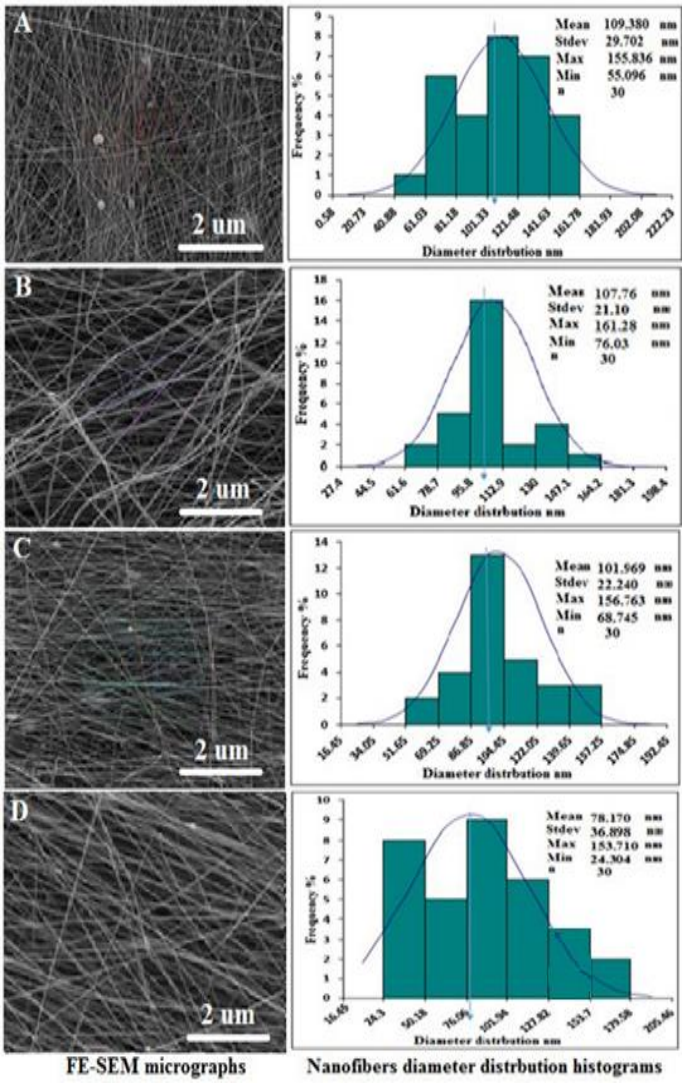

Fig.2 FE-SEM Micrographs and nanofibers diameter distribution histograms for (a) Pure PAN nanofibers, (b) 1.45 wt.%. γ- Fe_2O_3 nanofibers,(c) 4.30 wt.%. γ- Fe_2O_3 nanofibers, and (d) 7.14 wt.%. γ- Fe_2O_3 nanofibers

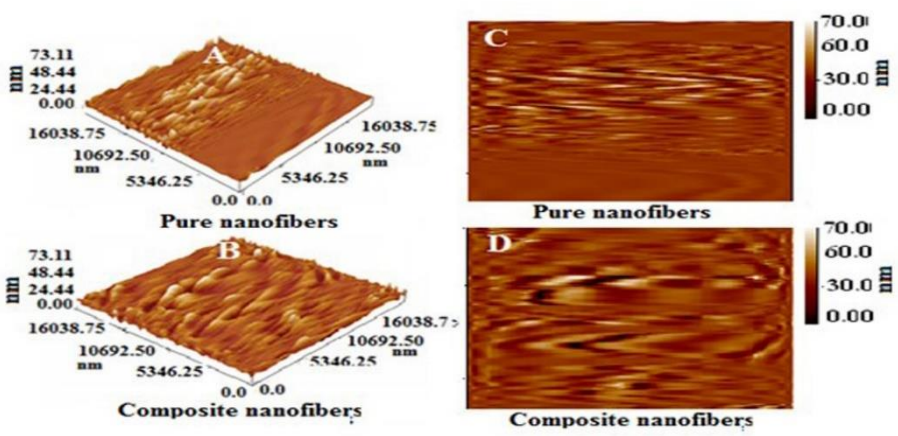

Fig .3 Shows the SPM imager surface roughness of 3D and 2D- micrographs AFM images for (A, C) Pure PAN nanofibers, (B, D) composite nanofibers.

Table .1 Results of surface nanofibers by using the SPM spectroscopy, mean surface area, and porosity %.

Sample of nanofibers	Ra (nm)	Rq (nm)	Rpv (nm)	Sdr (-)	Mean surface area (mm^2)	Porosity (%)
Pure PAN	3.670	6.160	70.50	0.518	168.50	50.0
PAN:Fe_2O_3	5.250	7.540	73.10	0.239	270.3	66.7

Ra = Average surface roughness, Rq = Root mean square surface roughness, Rpv = peak-to-valley roughness of the scanned region , and Sdr = Surface area ratio

3.2 Texture Direction and Porosity Properties

For determining the effect of magnetic properties of iron oxide nanoparticles on the alignment and the texture direction of pure nanofibers, we used the two-dimension–fast Fourier transforms (2D-FFT), which was calculated by ImageJ processing software (LOCI, University of Wisconsin). While we used the Mountains® 8 software (surface imaging, analysis, and metrology software) to plot, the texture direction curves dependent on the micrographs FE-SEM images. Fig. 4 (A-D) shows the change in the alignment direction, numbers, and size of gaps between the nanofibers with an increase in the wt.% of γ- Fe_2O_3 nanoparticles according to FE-SEM micrographs images . In addition to improvement in the orientation of alignment of the nanofibers measured by (2D-FFT) with increased amounts of iron oxide with orientation limits between 90˚ and - 90˚ as shown in Fig.4 (I-M). Furthermore, Fig. 4 (E-H) and Table 2 and show directionality histograms and the directionality analysis of the nanofiber's texture when changing from the orientation 81. 26° at the pure nanofiber to the orientation angle (- 3. 62°) at the 4.30 wt.% PAN: γ- Fe_2O_3 composite nanofibers, the dispersion of magnetics nanoparticles changing from dispersion 6 . 08° with a few amount 0. 28 while there is a major change in the orientation angle when adding a 4.30 wt. % PAN: γ- Fe_2O_3 the direction of composite nanofibers changing from 81. 26° to the -3. 62° with a change in the dispersion angle of magnetic nanoparticles from 6. 08° to 17. 85°, and an increase in the amounts of directed fiber with 62%, as well as the increase in the goodness of orientation nanofibers. The above results show the effect of the magnetic and electrical properties of the composite nanofibers on the alignment and directionality of texture nanofibers, as well as the increase in their surface area as shown in Table 1. Therefore, we observe the iron oxide nanoparticles lead to a decrease in the diameter of the nanofibers with an increase in the directionality and the isotropy percentage because the magnetic field decreases the diameter of the jet, which leads to a high control in the stability, and improves the kinetic energy of the jet [24].

In this study used the rotating drum with 900 rpm for production of 3-D nanofibers, the porosity percentage of these nanofibers was determined by the fluid displacement technique by immersing a suitable weight of nanofibers in 20 mL of ethanol in a graduated cylindrical bottle for 2 hours until saturating the submerged nanofibers with ethanol. The volume is then measured after immersion and the nanofibers are removed from the ethanol solution. The remaining volume is then measured. The porosity % was calculated according to the following equation [25].

Porosity % = $(V1 - V3)/(V2 - V3) * 100$ (1)

Where V_1 is volume of ethanol (mL), V_2 is volume with immersing the nanofibers after 2 hours (mL), and V_3 is the remaining volume after removing the nanofibers from the ethanol solution. It was observed that the porosity % increases with the presence of magnetic nanoparticles and that the porosity % depends on the reduction in the diameter of the nanofibers and that the porosity was 50 % at (109.380 ± 29.702 nm) of the pure PAN nanofibers, while the porosity % became 67. 67 % for the composite fibers at (78.170 ± 36.898 nm). The decrease in the average nanofiber diameters led to an increase in the density of the deposited nanofibers on the rotating collector. These results led to a reduction in the numbers and the size of the spaces (gaps) between the nanofibers and an increase in the porosity % as shown in Fig. 4 (C, D). Compare with a decrease in the density of the nanofibersm and an increase in the numbers and size of the spaces (gaps) between the nanofibers in Fig. 4(A, B) [26, 27] .

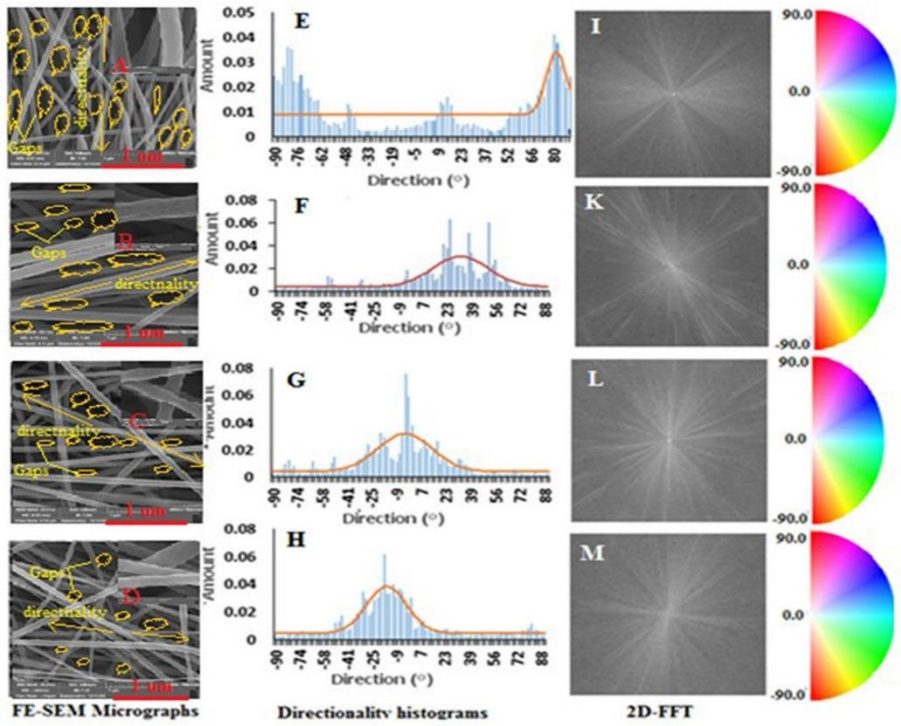

Fig.4 FE-SEM Micrographs, Directionality histogram, and 2D-FFT for (A,E,I) Pure PAN nanofibers, (B,F,K) 1.45 wt. %.γ- Fe_2O_3 nanofibers, (C,G,L) 4.30 wt. %.γ- Fe_2O_3 nanofibers, and (D,H,M) 7.14 wt. %. γ- Fe_2O_3 nanofibers

3.3 UV- Visible and Fourier transform Analysis

In order to strengthen the PAN nanofibers, make them more porous, and have a larger surface area, the iron oxide nanoparticles were added to determine the optical properties of the nanofibers based on the absorption spectra versus the wavelength obtained using (UV-Visible) spectrophotometer. Fig. 5 shows the analysis of the absorption spectrum against the wavelength of the elements in the pure and composite nanofibers. The absorption edge at the wavelength is 362 nm for pure nanofibers and 383 nm for composite nanofibers, while the maximum absorption edge is 270, and 285 nm for pure and composite nanofibers respectively. On the other hand, the spectral absorption edge increased from 0.63 for pure nanofibers to 3.84 for composite nanofibers . The result is due to the effect of adding nanoparticles of iron oxide [27].

Used the Fourier transform Near-infrared spectroscopy (FT-NIR) analysis with range (450-4000) cm^{-1} to identify the molecular characterization and discover the chemical bonds that occur through the formation of composite nanofibers. Fig. 6 illustrates the absorption peaks for pure nanofibers are (522,1042, 1235,1372,1452, 1666, 1737, 2242, 2936, 3625) cm^{-1} respectively, the peak at 2936 cm^{-1} indicates the vibration stretching of methylene (-CH_2-) in addition to the peaks at 2242 and 1452 cm^{-1}. It led to stretch vibration of the nitrile group (-CN-) and bending vibration of (-CH_2-). On the other hand, we note that the peak at 1666 cm^{-1} indicated the surfactant of the γ- Fe_2O_3 nanoparticles [12, 28]. For composite nanofibers , the stronger peaks were at 2936 cm^{-1} (CH stretching) and 1452 cm^{-1} (CH bending) according to CH and CH2. In addition, we notice a peak for PAN: γ- Fe2O3 at 478 cm^{-1} allowed the network vibration of

iron oxide nanoparticles, which led to the formation of γ- Fe_2O_3 set onto the PAN nanofiber surface [29].

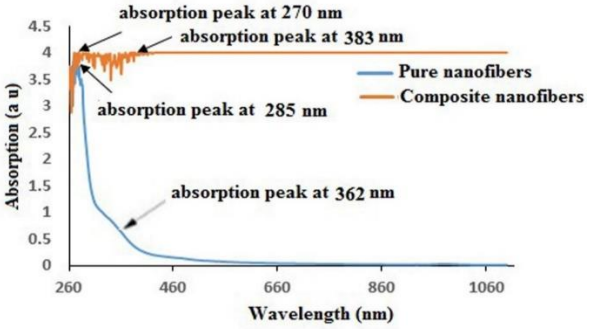

Fig.5 UV-Vis spectrum for pure and composite nanofibers.

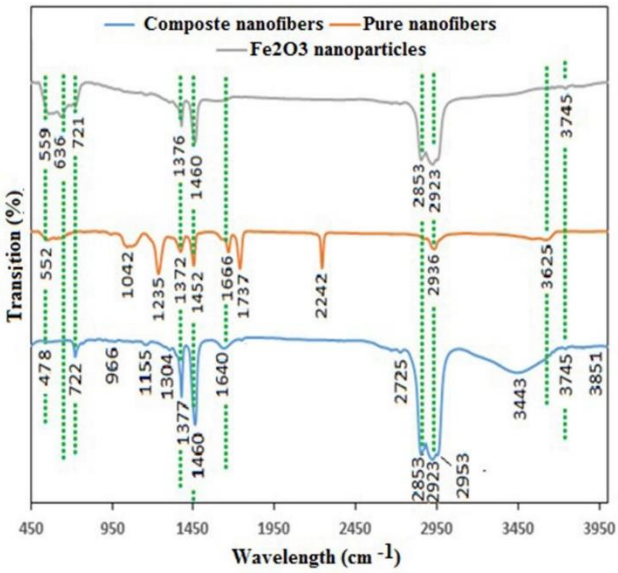

Fig. 6 Fourier transform near-infrared spectroscopy (FT-NIR) analysis for γ- Fe_2O_3 nanoparticles, pure, and composite nanofibers

3.4 Crystalline Properties

Crystalline properties are one of the most important physical properties to determine the efficiency of pure nanofibers and nanofibers strengthened by iron nanoparticles for many engineering application as absorbing the heavy metal ions. Therefore, we used the (Philips PAN analytical –X'Pert HighScore Plus) to measure crystalline properties such as crystalline size and crystallinity %, as well as Herman's orientation function (f) to orient the polymer chains. Fig. 7 shows X-ray scattering of pure nanofibers and PAN: γ- Fe_2O_3 nanofibers with different γ- Fe_2O_3 loading (1.45, 4.3, 7.14) wt.% respectively. All samples have the peaks such as 2θ ≈17°, 28°,35.3°, and 50.5°, while the peaks 2θ≈60.8° at nanofibers loading with 1.43, 4.3, and 7.14 wt. % γ- Fe_2O_3 and peak 2 θ ≈63°, 71.5°, and 74,9° at 7.14 wt.% γ- Fe_2O_3 . According to the results above, we note that the strong peaks for PAN nanofibers at 2θ ≈17°. While strong peaks were formed after adding the iron oxide nanoparticle, especially at 1.43, 4.3, and 7.14 wt.% such as 2θ ≈35.5° and 43.3° , a strong peak was also found at 7.14 wt.% as 63.07° . These results indicated the high interaction between iron oxide nanoparticles and polymer matrix [28, 29]. On the other hand, it is possible to use (Bragg's Law) to calculate (d- spacing) according to equation:

$$d = n\lambda/(2\,sin\theta) \quad (2)$$

Where n is chosen as 1 and λ is 1.5406 Å for the wavelength of Cu Ka radiation. According to the above equation, d spacings are 5.41 Å and 3.667 Å for 2θ≈ 17° and 24.3°, respectively. The average crystalline size (D) was calculated from the Debye–Scherrer equation:

$$D = k\lambda/\beta(2\theta)cos\theta \quad (3)$$

Where β (2θ) is the full width at half of the maximum (FWHM), K is a constant with a value of 0.9, and θ is the Bragg angle and the average crystal size is calculated only at 2θ≈ 17°.

The crystalline orientation of polymer chains can be estimated by Herman's orientation function (f) according to following equation [3, 10].

$$f=\frac{1}{2}(3 *< \ cos^2\theta \ >) - 1 \quad (4)$$

Where (Ø) is the angle between the x-axis of the polymeric chain and the plane (101), the square average cos (Ø) is defined according to the following equation.

$$< cos^2\theta \geq = \ cos^2\theta < cos^2\beta \ \geq =$$
$$cos^2\theta \int_0^{\frac{\pi}{2}} I(\beta) sin\beta cos^2\beta d\beta / \int_0^{\frac{\pi}{2}} I(\beta) sin\beta d\beta \quad (5)$$

Where $I(\beta)$ is the intensity profile along with the azimuthal angle ,β is the azimuthal angle, and θ is Bragg's angle . The value of f is 1 and -0.5, meaning the polymer chains are aligned either perfectly parallel or perpendicular to the fiber axis. In addition, if f is zero, the nanofibers are randomly oriented' [30]. The results of the X-ray analysis showed that all the samples have two tropical peaks, one at 2θ≈ 17° dependent on the d- spacing (d≈ 5.33 Å) from the (100) reflection and the other at 2θ≈ 28° depending on the d-spacing (3.20 Å) from the (110) (equation 2) , therefore the ratio between the two peaks' d-spacing is approximately 1. 74, which indicated that the PAN chains are hexagonally packed. On the other hand, Table 3 shows the results of crystalline properties such as crystallinity %, average crystalline size, and the Herman orientation function for polymer chains. In the other words, we note that a convergence in the results achieved in Table 2 and Table 3 regarding the influence of the orientation angle of the composite nanofibers in Table 2 by the iron oxide nanoparticles loaded and the influence of Herman orientation factor for crystalline orientation of polymer chains with those particles in Table 3. Therefore, the crystalline properties are directly affected by iron oxide nanoparticles [31] .

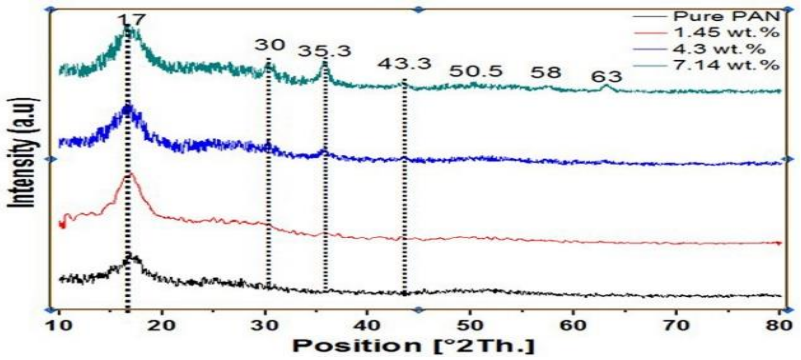

Fig. 7. XRD patterns of pure nanofibers and PAN: γ- Fe_2O_3 nanofibers with different Fe_3O_4 loading: (1.45, 4.3, 7.14) wt. % respectively

Table 2 Results of directionality analysis for pure and composite nanofibers (using Fourier components)

Samples of nanofibers	Direction(°)	Dispersion (°)	Amount	Goodness
Pure PAN	81.26	6.08	0.28	0.35
1.45 wt. %. Fe_2O_3	32.20	18.60	0.74	0.54
4.30 wt. %. Fe_2O_3	-3.62	17.85	0.74	0.59
7.14 wt. %. Fe_2O_3	-15.53	13.52	0.66	0.84

Table 3 The results of crystalline properties for the pure and composites nanofibers.

Samples	Average Crystalline Size (nm)	Crystallinity (%)	Herman Orientation Factor
Pure Nano fibers	6.50	82.43	-0.248
1.45 wt.% γ-Fe_2O_3	10.60	83.73	-0.230
4.30 wt.% γ-Fe_2O_3	12.40	94.28	-0.413
7.14 wt.% γ- Fe_2O_3	18.40	88.48	-0.500

3.5 Thermal Behavior

Differential calorimeter scanning (Netzsch DSC) was used to characterize the thermal properties of electrospun pure PAN and PAN: γ- Fe_2O_3 composite nanofibers as shown in Fig. 8. The DSC thermographs showed the change in the thermal behavior of the pure nanofibers after adding the nanoparticles of iron oxide. The glass transition temperature (Tg) increased from 106.91C in the case of pure nanofibers to 111.91C in the case of composite nanofibers, with an increase of 4%, while the area of thermal diffusion increased from (-2475) J/ g to (-3599) J/ g, with an increase of 31.23%. On the other hand, we note that the DSC thermographs showed that the pure nanofiber has a crystallization peak at 321.2 C, while the composite nanofiber has two crystallization peaks, one at 319 C and the other sharp peak at 351.8 C because of the melting peak of γ- Fe_2O_3 filled PAN fibers [32]. The change in thermal behavior is attributed to the activity of iron oxide particles by reducing the mobility polymer chains and increasing the Tg . The morphological tests showed a decrease in the diameter of the nanofibers with improvement in the directionality of the texture, as well as increasing the crystallization properties, which were proven by means of XRD and FTR tests [32- 34].

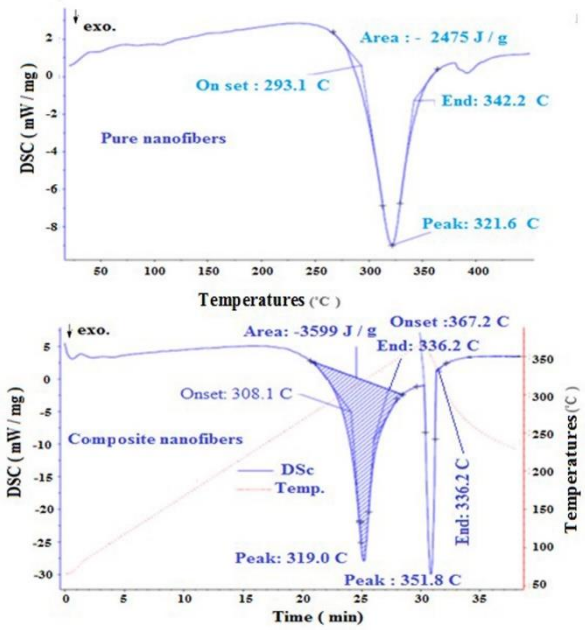

Fig.8 NETZSCH DSC thermographs for pure and composite nanofibers

3.6 Magnetic Properties

The magnetic properties of the materials used for reinforcement of pure nanofibers depend on the geometrical shape, size, and thickness of the particles, which in turn are reflected in the morphological properties of the composite nanofibers such as the

diameter and orientation of the fiber, in addition to the crystalline, thermal, and rheological properties [12, 24, 32]. To determine the above properties, especially for the thin films such as nanofibers, the vibrating-sample magnetometer (VSM) was used to determine the saturation magnetization (Ms), remnant magnetization (Mr), and coercivity (Hc). Table 4 and Fig. 9 illustrate the results and magnetic behavior of pure and composite fibers through the hysteresis loop (M-H). From Fig. 9a , we notice that the saturation magnetization (Ms) increases with the increase of iron oxide loading in the nanofibers, as it increases from (1.426 emu/g) at 1.45 wt.% γ- Fe_2O_3 to (6.85 emu/g) for composite nanofibers at 7.14 wt.% γ Fe_2O_3. On the other hand, we note that coercivity (Hc) increases proportionally with an increase in loading iron oxide nanoparticles, which represented the intersection of the external magnetic field (horizontal axis) with the magnetization (vertical axis). The remnant magnetization (Mr) also increases proportionally, which represented the re-magnetization to the zero points by the external magnetic field. Two characteristics determine the efficiency of the magnetic strength of the composite nanofibers (see in Fig. 9b). In addition, the remanence ratio (MR/MS) gives an impression of good diffusion and non-aggregating of iron oxide nanoparticles in the polymeric matrix. Therefore, the lowest remanence ratio was 0.029 at 1.45 wt.% γ- Fe_2O_3, while the highest remanence ratio was 0.036 for composite fibers at 7.14 wt. % γ- Fe_2O_3 [35- 37] .

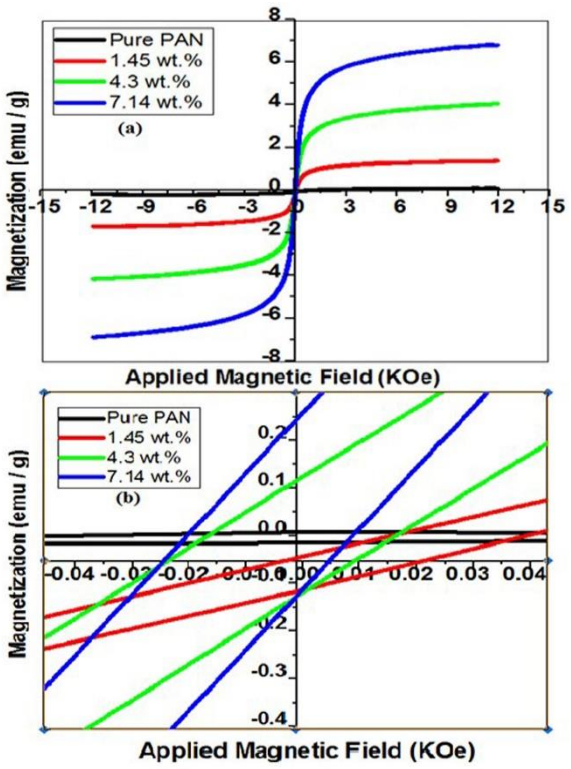

Fig.9 (M-H) Hysteresis loops performed on samples at room temperature for (a) the range of applied magnetic field between the ± 15 (KOe), (b) low applied magnetic field between ± 0.04 (KOe)

Table 4 Results of the vibrating-sample magnetometer (VSM) such as Saturation magnetization (Ms), remnant magnetization (Mr), and the coercivity (Hc)

Samples	MS (emu/g)	Mr (emu/g)	Hc (Oe)	Mr : Ms
1.45 wt.% PAN : γ- Fe_2O_3 nanofibers	1.426	0.041	119	0.029
4.3 wt.% PAN :γ- Fe_2O_3 nanofibers	4.156	0.127	128	0.031
7.14 wt.% PAN : γ- Fe_2O_3 nanofibers	6.854	0.249	130	0.036

(Ms) is a Saturation magnetization, (Mr) is a remnant magnetization, and (Hc) is a coercivity , Oe: oersted

Conclusion

The γ- Fe_2O_3 nanoparticles played an important role in improving the physical characteristics of the 3D pure PAN nanofibers, which made them more porous, changing the directionality of nonwoven textile nanofibers. Indention excellently controlled the formation of the beads and increased the density of the deposited fibers on the collector as a result of the decrease in the diameter of the nanofiber and improvement of the magnetic properties with the increase in the amount of iron oxide. This behavior was positively reflected in the improvement of the crystalline properties and the increase of the Hermann's factor, which played an important role in orientation the polymer chains. Increases the interaction between iron oxide particles and the polymer matrix through using FE-SEM, AFM, XRD, FT-NIR, and VSM analysis, which reflect the expansion of' the engineering applications such as treatment of water contaminated with heavy metal ions.

Acknowledgments

The authors of this research are very grateful for the services proofreading provided by Mr. James Morgan from Twin English Centre London, 12 Lambarde Square Greenwich, and London SE10 9GB-United Kingdom. In addition, the Laboratory of Polymer Engineering and Petrochemical Industries at the University of Babylon, as well as the services provided by the companies ARYA Electron Optic Company –

Iran, and XRD Laboratory - University of Kashan - Iran to conduct laboratory tests.

Declaration of Interest Statement

The authors declare that they have no known competing financial interests or personal relationships that could have appeared to influence the work reported in this paper.

Conflict of interests

The Author(s) declare(s) that there is no conflict of interest.

References

[1] Haider S and Park S.Y, Preparation of the electrospun chitosan nanofibers and their applications to the adsorption of Cu (II) and Pb (II) ions from an aqueous solution , J. Membr. Sci , 328(1-2),90-96 (2009).

[2] Faris D, Hadi N.J and Habeeb S.A, In Proceedings of the 3rd International Conference on Materials Engineering & Science: Effect of rheological properties of (Poly vinyl alcohol/Dextrin/Naproxen) emulsion on the performance of drug encapsulated nanofibers. Materials Today: Proceedings, 42(5), 2725-2732 (2021). doi.org/10.1016/j.matpr.2020.12.712

[3] Habeeb S.A, Rajabi L and Dabirian F. Comparing Two Electrospinning Methods in Producing Polyacrylonitrile Nanofibrous Tubular Structures with Enhanced Properties, Iran. J. Chem. Chem. Eng. (IJCCE), 38(3), 23-42(2019).

[4] Habeeb S.A, Rajabi L and Dabirian F. Production of polyacrylonitrile/boehmite nanofibrous composite tubular structures by opposite-charge electrospinning with enhanced properties from a low-concentration polymer solution, Polym. Compos, 41(4), 1649-1661 (2020).

[5] Alobad Z.K, Habeeb S.A and Albozahid M.A. A Review on Silicone Rubber / Montmorillo-Nite Nano composites , The Iraqi Journal for Mechanical and Materials Engineering , 20(3),268-281 (2020).

[6] Habeeb S.A, Alobad Z.K and Albozahid M.A. The effecting of Physical Properties of Inorganic Fillers on Swelling Rate of Rubber Compound: A review Study, J. Univ. Babylon eng. Sci. , 27(1),94-104 (2019).

[7] Habeeb, S.A., Diwan, A., Albozahid, M. A, Compressive Review on Swelling Parameters and Physical Properties of Natural Rubber Nano composites, Egypt. J. Chem, 2021; (Article in press),doi: 10.21608/ejchem.2021.72560.3613

[8] Albozahid, M., Diwan, A., Habeeb, S.A. The Effect of Addition Graphite Filler on Mechanical Properties of Epoxy Material. Egypt. J. Chem, 2021, (Article in press), doi: 10.21608/ejchem.2021.73645.3638

[9] Zhang L, Luo J, Menkhaus T.J, Varadaraju H, Sun Y and Fong H, Antimicrobial nano-fibrous membranes developed from electrospun polyacrylonitrile nanofibers, J. Membr. Sci. , 369 (1-2),499-505 (2011).

[10] Zhang D, Karki A.B, Rutman D, Young D.P, Wang A, Cocke D, Ho T.H and Guo Z, Electrospun polyacrylonitrile nanocomposite fibers reinforced with Fe3O4 nanoparticles: Fabrication and property analysis, Polymer, 50(17),4189-4198 (2009).

[11] Liu H, Zhang Z.G, Wang X.X, Nie G.D, Zhang J, Zhang S.X, Cao N, Yan S.Yand Long Y.Z. Highly flexible Fe_2O_3 /TiO2 composite nanofibers for photocatalysis and utraviolet detection, J. Phys. Chem. Solids ,121 ,236-246 (2018).

[12] Jafari M, Salehi M and Behzad M, Structural, magnetic and electrical properties of pure and Dy-doped Fe_2O_3 nanostructures synthesized using chemical thermal decomposition technique, Int J Nano Dimens , 9(2),179-190 (2018).

[13] Park C.H, Kang S.J, Tijing L.D, Pant H.R and Kim C.S, Inductive heating of electrospun Fe_2O_3 /polyurethane composite mat under high-frequency magnetic field .Ceram. Int , 39(8):9785-9790 (2013).

[14] Kim Y.J, Liu Y.D, Seo Y and Choi H.J, Pickering-emulsion-polymerized polystyrene/ Fe_2O_3 composite particles and their magnetoresponsive characteristics, Langmuir , 29(16),4959-4965 (2013).

[15] Jung Y, Barry M, Lee J.K, Tran P, Soong Y, Martello D and Chyu M , Effect of nanoparticle-additives on the rheological properties of clay-based fluids at high temperature and high pressure. In AADE national technical conference and exhibition. Houston, TX: American Association of Drilling Engineers , 1-4 (2011).

[16] Albozahid M, Habeeb S.A, Alhilo N.A and Saiani A, The impact of graphene nanofiller loading on the morphology and rheology behaviour of highly rigid polyurethane copolymer, Mater. Res. Express, 7(12), 125304 (2020).

[17] Phuoc T.X and Massoudi M, Experimental observations of the effects of shear rates and particle concentration on the viscosity of Fe2O3–deionized water nanofluids, Int J Therm Sci , 48(7),1294-1301 (2009).

[18] Gai G, Wang L, Dong X, Zheng C, Yu W, Wang J and Xiao X, Electrospinning preparation and properties of magnetic-photoluminescent bifunctional bistrand-aligned composite nanofibers bundles, J Nanopart Res ,15(4),1539 (2013).

[19] Chen Y, Zhao X, Liu Y, Razzaq A.A, Haridas A.K, Cho K.K, Peng Y, Deng Z and Ahn J.H, γ-

Fe_2O_3 nanoparticles aligned in porous carbon nanofibers towards long life-span lithium ion batteries, Electroch

[20] Song C, Wang X.X, Zhang J, Nie G.D, Luo W.L, Fu J, Ramakrishna S and Long Y.Z, Electric field-assisted in situ precise deposition of electrospun γ- Fe_2O_3 /polyurethane nanofibers for magnetic hyperthermia, Nanoscale Res Lett , 13(1):1-11(018).

[21] Zheng J, Sun B, Wang X.X, Cai Z.X, Ning X, M Alshehri S, Ahamad T, Xu X.T, Yamauchi Yand Long Y.Z. Magnetic-Electrospinning Synthesis of γ- Fe_2O_3 Nanoparticle–Embedded Flexible Nanofibrous Films for Electromagnetic Shielding, Polymers, 12(3),695 (2020).

[22] Habeeb S.A. Enhancing the Properties of Styrene-Butadiene Rubber by Adding Borax Particles of Different Sizes, Iran. J. Chem. Chem. Eng. (IJCCE) 2020, https://dx.doi.org/10.30492/ijcce.2020.40535

[23] Ray S.S, Chen S.S, Li C.W, Nguyen N.C and Nguyen H.T, A comprehensive review: Electrospinning technique for fabrication and surface modification of membranes for water treatment application, RSC Adv , 6(88),85495-85514 (2016).

[24] He J.H, Liu Y, Mo L.F, Wan Y.Q and Xu L, Electrospun nanofibres and their applications. Shawbury, UK: ISmithers , 2008.

[25] Fallahiarezoudar E, Ahmadipourroudposht M, Yusof N.M, Idris A and Ngadiman N.H, 3D biofabrication of thermoplastic polyurethane (TPU)/poly-L-lactic acid (PLLA) electrospun nanofibers containing maghemite (γ- Fe_2O_3) for tissue engineering aortic heart valve, Polymers , 9 (11),584 (2017).

[26] Zhao R, Li X, Li Y, Li Y, Sun B, Zhang N, Chao S and Wang C, Functionalized magnetic iron oxide/polyacrylonitrile composite electrospun fibers as effective chromium (VI) adsorbents for water purification, J. Colloid Interface Sci , 505,1018-1030 (2017).

[27] Liu H, Zhang Z.G, Wang X.X, Nie G.D, Zhang J, Zhang S.X, Cao N, Yan S.Y and Long Y.Z, Highly flexible Fe2O3/TiO2 composite nanofibers for photocatalysis and utraviolet detection, J. Phys. Chem. Solids, 121,236-246 (2018).

[28] Chang J, Wang J, Qu J, Li Y.V, Ma L, Wang L, Wang X and Pan K, Preparation of α-Fe 2 O 3/polyacrylonitrile nanofiber mat as an effective lead adsorbent, Environ. Sci. Nano, 3(4), 894-901 (2016)

[29] Gao Q, Luo J, Wang X, Gao C and Ge M, Novel hollow α- Fe_2O_3 nanofibers via electrospinning for dye adsorption, Nanoscale Res Lett ,10 (1):1-8 (2015).

[30] Yano T, Higaki Y, Tao D, Murakami D, Kobayashi M, Ohta N, Koike J.I, Horigome M, Masunaga H, Ogawa H and Ikemoto Y. Orientation of poly (vinyl alcohol) nanofiber and crystallites in non-woven electrospun nanofiber mats under uniaxial stretching, Polymer, 53 (21),4702-4708 (2012).

[31] Song Z, Hou X, Zhang L and Wu S, Enhancing crystallinity and orientation by hot stretching to improve the mechanical properties of electrospun partially aligned polyacrylonitrile (PAN) nanocomposites. Materials, 4 (4), 621-632 (2011).

[32] Dhanote A, Ugbolue S.C, Warner S.B, Patra P.K, Katangur P and Mhetre SK. Solution Electrospinning of Nylon/Ferrite Nanofibers, MRS Online Proceedings Library ,788(1),8451-8456 (2003).

[33] Shahrousvand M, Hoseinian M.S, Ghollasi M, Karbalaeimahdi A, Salimi A and Tabar F.A, Flexible magnetic polyurethane/ Fe_2O_3 nanoparticles as organic-inorganic nanocomposites for biomedical applications: Properties and cell behaviour, Mater. Sci. Eng. C , 74, 556-567 (2017).

[34] Kausar A, Polymeric materials filled with hematite nanoparticle: current state and prospective application, Polym Plast Technol Eng , 59(3),323-338 (2020).

[35] Bellucci F.S, de Almeida F.C, Nobre M.A, Rodríguez-Pérez M.A, Paschoalini A.T and Job A.E, Magnetic properties of vulcanized natural rubber nanocomposites as a function of the concentration, size and shape of the magnetic fillers, Compos Part B-Eng, 85,196-206 (2016).

[36] Kumar S, Singh R, Singh T.P and Batish A, Investigations for magnetic properties of PLA-PVC- Fe_2O_3-wood dust blend for self-assembly applications, J. Thermoplast. Compos. Mater, 0892705719857778 (2020).

[37] Zhang X, Pan W, Dong J, Liu Q and Wang J, Fabrication and characterization of FePt magnetic nanofibers via electrospinning technique, J. Mater. Sci, 50 (22), 7218-7226 (2015).